



Tailoring polarisation of attosecond pulses via co-rotating bicircular laser fields

Rambabu Rajpoot ^{1,*}, Amol R. Holkundkar ^{1,†}, Navdeep Rana,² and Gopal Dixit²

¹*Department of Physics, Birla Institute of Technology and Science - Pilani, Rajasthan, 333031, India.*

²*Department of Physics, Indian Institute of Technology Bombay, Powai, Mumbai, 400076, India.*

(Dated: May 2, 2023)

The present work introduces a robust way to generate attosecond pulses with tunable ellipticity via high-order harmonic generation by co-rotating $\omega - 2\omega$ bicircular laser fields. The total electric field of the laser fields exhibits an absence of rotational symmetry, which leads to the generation of high harmonics of the same helicity across a broad range of spectral bandwidth. High-harmonics with the same helicity offer the opportunity to synthesize attosecond pulses with tunable ellipticity. The polarisation properties of the generated harmonics are robust against the variations in driving fields' parameters, such as wavelength, intensity ratio, and the sub-cycle phase between $\omega - 2\omega$ fields. Our work opens an avenue to study chiral-sensitive light-matter ultrafast processes on their intrinsic timescale.

I. INTRODUCTION

High-harmonic generation (HHG) is one of the non-perturbative nonlinear processes of laser-matter interaction. HHG has been intensively used for a tabletop coherent light source in extreme ultraviolet and soft x-ray energy regimes with attosecond temporal resolution [1]. HHG in a gaseous medium proceeds via a three-step process [2, 3], wherein an intense laser pulse liberates an electron via tunnel ionisation as a first step. The liberated electron gains energy in the presence of driving laser as it propagates in the continuum and, eventually, is driven back to recollide with the parent ion. The kinetic energy acquired by the electron is emitted in the form of higher-order harmonics of the driving laser field. HHG not only plays a paramount role in producing attosecond pulses, but also offers a wide array of applications by unraveling ultrafast electron dynamics in matter with atomic-scale spatial-temporal resolutions [4–10].

Owing to the rapid development on both the theoretical and experimental fronts, researchers have focused on controlling the polarization of the emitted harmonics. Usually, the polarization of the emitted harmonics is controlled by utilizing various forms of the counter-rotating $\omega - 2\omega$ bicircular fields configuration, such as fields having different intensity ratios, relative phase, and ellipticities [11–20], non-collinear mixing of combining pulses [21, 22], adding a seed pulse [23], as well as utilizing the plasmonic field enhancement [24], to name a few. However, due to the three-fold symmetry restriction enforced by the counter-rotating $\omega - 2\omega$ fields, harmonics with alternating helicity are generated. Such circularly polarized harmonics with alternating helicity could generate linearly polarized attosecond pulses with each subsequent pulse rotated by 120° in space [25]. Thus, it is crucial to desire harmonics of the same helicity across a range of spectral bandwidths to produce attosecond pulse with tunable ellipticity.

In this work, we introduce a robust scheme to generate attosecond pulse with tunable ellipticity using co-rotating $\omega - 2\omega$ circularly polarized fields. In the following, we will

demonstrate that the harmonics with the same helicity are produced owing to the absence of rotational symmetry in the driving co-rotating $\omega - 2\omega$ bicircular fields. The robustness of our scheme is tested with respect to the variations in the driving fields' parameters. It is found that highly elliptical attosecond pulse can be generated as the scheme is insensitive to any variations in the parameters. The generated attosecond pulses with circular or elliptical polarization are desirable to probe various chiral-sensitive light-matter phenomena [26–32]. Recently, Lu and co-workers have applied corotating bicircular field configurations with 1:3 ratio to discuss the role of Coriolis-force effect in the generation of high harmonics [33]. Moreover, the superiority of the molecular target over atomic in the context of corotating bicircular fields setup is discussed in Ref. [34]. Solids and plasma targets, apart from gaseous systems, have also attracted attentions for HHG via co-rotating driving fields [35–37].

The paper is organized as follows. Details of the numerical methods are discussed in Sec. II, followed by the results and discussion in Sec. III. The concluding remarks and future directions are discussed in Sec. IV.

II. NUMERICAL METHODS

Time-dependent Schrödinger equation in two-dimensions, within single-active-electron approximation, for helium is numerically solved as discussed in Refs. [16, 38]. The harmonic spectrum is obtained by performing the Fourier transform of the dipole acceleration as

$$S_\kappa(\Omega) = \left| \frac{1}{\sqrt{2\pi}} \int a_\kappa(t) e^{-i\Omega t} dt \right|^2 = |a_\kappa(\Omega)|^2, \quad (1)$$

where κ stands for the x or y components of the time-dependent dipole acceleration. To describe the polarization of the harmonics, the intensity of the left- and right-rotating components is obtained as $D_\pm = |a_\pm(\Omega)|^2$ with $a_\pm(\Omega) = [a_x(\Omega) \pm ia_y(\Omega)]/\sqrt{2}$. Ellipticity of the emitted harmonics is calculated using

$$\varepsilon = \frac{|a_+(\Omega)| - |a_-(\Omega)|}{|a_+(\Omega)| + |a_-(\Omega)|}. \quad (2)$$

* E-mail: ramrajpoot3@gmail.com

† E-mail: amol@holkundkar.in

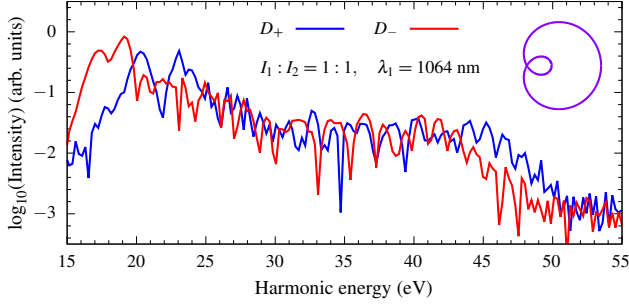


FIG. 1. High-harmonic spectrum of helium driven by co-rotating $\omega - 2\omega$ fields. D_+ harmonic component (blue line) is co-rotating with the ω field, whereas the red line represents the counter-rotating D_- harmonic component. Inset shows Lissajous figure corresponding to the total co-rotating $\omega - 2\omega$ electric fields for one cycle of ω_1 field. $\lambda_1 = 1064$ nm, $I_1 = I_2 = 5 \times 10^{13}$ W/cm², and $\phi = 0^\circ$ are used to simulate the spectrum.

The parameter ε varies in the interval from -1 to $+1$, and the sign of ε defines the helicity of the harmonics. The harmonics rotating in a counter-clockwise direction have positive helicity while those rotating in a clockwise direction have negative helicity [39, 40].

The temporal profile of an attosecond pulse is constructed by filtering the desired frequency range with an appropriate window function $w(\Omega)$ and then performing an inverse Fourier transform as [41]:

$$\mathcal{E}_\kappa(t) = \frac{1}{\sqrt{2\pi}} \int a_\kappa(\Omega) w(\Omega) e^{i\Omega t} d\Omega. \quad (3)$$

Here, $w(\Omega) = \Theta(\Omega - \Omega_1)\Theta(\Omega_2 - \Omega)$, wherein $\Omega_1 \leq \Omega \leq \Omega_2$ is the frequency range to be filtered, and $\Theta(x)$ is standard step function.

The total electric field corresponding to the $\omega - 2\omega$ co-rotating configuration is written as

$$\mathbf{E}(t) = f(t) \left\{ E_1 [\cos(\omega_1 t) \hat{\mathbf{e}}_x + \sin(\omega_1 t) \hat{\mathbf{e}}_y] + E_2 [\cos(\omega_2 t + \phi) \hat{\mathbf{e}}_x + \sin(\omega_2 t + \phi) \hat{\mathbf{e}}_y] \right\}, \quad (4)$$

where ω_j and E_j are the frequency and the electric field amplitude of the j^{th} component of the bicircular field, respectively. ϕ defines the sub-cycle phase between the two fields. The temporal pulse envelope $f(t) = \sin^2(\pi t/\tau)$ with total duration $\tau = 5T_1$, where $T_1 = 2\pi/\omega_1$ is the period of the fundamental field.

We have considered the spatial simulation domain of ± 150 a.u. along both x and y directions. The value of parameter $r_{\text{abs}} = \pm 142$ a.u. is considered. The spatial step $\Delta x = \Delta y \approx 0.29$ a.u. is used and the simulation time step $\Delta t = 0.01$ a.u. is considered, which is well within the criteria $\Delta t \lesssim 0.5(\Delta x)^2$. The convergence is tested with respect to the spatial grid as well as space and time steps. Our simulation utilizes widely used *Armadillo* library for linear algebra purpose [42].

In the following sections, we discuss the harmonic generation by co-rotating bicircular laser pulses and the production of highly elliptically polarized attosecond pulses.

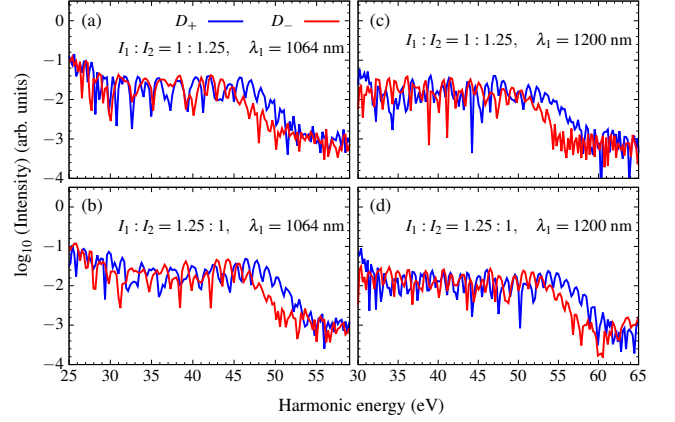


FIG. 2. Same as Fig. 1 with different wavelengths, and intensity ratios. The wavelength is considered 1064 nm in (a-b) and 1200 nm in (c-d). Here, value 1 corresponds to the intensity 5×10^{13} W/cm².

III. RESULTS AND DISCUSSIONS

The harmonic spectra of helium driven by co-rotating $\omega - 2\omega$ fields is presented in Fig. 1. Absence of the dynamical rotational symmetry of the total electric field results in the generation of even and odd-order harmonics with a regular plateau structure as evident from the figure. Additionally, the harmonic component co-rotating with the driving field has higher contrast, dominates in the cutoff region. The present observations are consistent with the propensity rules as discussed in Ref. [43]. This is in contrast with counter-rotating $\omega - 2\omega$ configuration, which results in harmonic doublets with alternating helicity.

Before we discuss the generation of attosecond pulses with tunable ellipticity from the spectrum shown in Fig. 1, let us explore the robustness of the features in the spectrum with respect to various laser parameters. Figure 2 presents harmonic spectra corresponding to co-rotating $\omega - 2\omega$ configuration having different fundamental wavelengths and intensity ratios. The overall nature of the spectrum remains insensitive with respect to the changes in the intensity ratio as the ratio is tuned from 1:1 to 1:1.25 and 1.25:1, as evident from Figs. 2(a) and 2(b), respectively. A similar observation can be made when the wavelength is increased from 1064 nm to 1200 nm with the same intensity ratios [see Figs. 2(c) and 2(d)]. Thus, the higher yield of the co-rotating harmonic component in blue is insensitive with respect to the variations in the wavelength as well as intensity ratio of the co-rotating fields. In all cases, the subcycle phase between $\omega - 2\omega$ fields, ϕ , is zero. At this juncture, it is natural to envision how different values of ϕ affect the nature of the harmonic spectra discussed so far.

Figure 3 presents harmonic spectra for different values of ϕ for 1200 nm wavelength of ω -field with 1:1 intensity ratio. As the value of ϕ is tuned from $\phi = 0^\circ$ to $\phi = 30^\circ$, spectrum shown in Fig. 3(a) displays high contrast of the D_+ harmonic component, co-rotating with the driving field, compared to the counter-rotating D_- harmonic component in the cutoff region. The insensitivity of the features of the harmonic spectra can

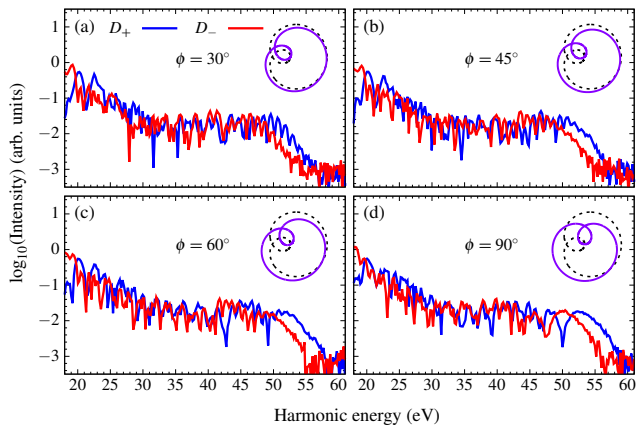


FIG. 3. Sensitivity of the harmonic spectra with respect to the sub-cycle phase, ϕ , between $\omega - 2\omega$ fields. (a) 30° , (b) 45° , (c) 60° , and (d) 90° . Insets show Lissajous figures corresponding to co-rotating driving fields (solid purple line) with the Lissajous figure for $\phi = 0^\circ$ in a black dotted line for comparison purposes. $\lambda_1 = 1200$ nm, and $I_1 = I_2 = 5 \times 10^{13}$ W/cm² are used to simulate the spectra.

be understood by analysing the Lissajous figure. The orientation of the Lissajous figure rotates by changing ϕ value, but dynamical rotational symmetry is still absent, as visible from the inset. As a result, the polarization and intensity of the emitted harmonics remain unaffected for different values of ϕ , as evident from the spectra shown in Figs. 3(b) - 3(d).

We have also simulated the harmonic spectra when the helicity of the co-rotating driving fields is reversed. In this case, the co-rotating harmonic component dominates in the cutoff region regardless of the rotation direction of the driving field as can be seen in Fig. 4. This offers the possibility of generating attosecond pulses with desired handedness by simply changing the rotation direction of the driving laser pulses.

From the analysis of Figs. 1 - 3, it is established that the essential features of the harmonic spectra, such as domination of the co-rotating D_+ component, are robust with respect to the variations in the laser parameters. This eliminates the need for precise adjustments of the intensity ratio or the relative phase between the driving fields or a specific choice of wavelength. Thus, co-rotating $\omega - 2\omega$ scheme can be utilized to synthesize attosecond pulse with controlled polarization.

To illustrate the feasibility of generating attosecond pulses with tunable polarization via HHG driven by co-rotating $\omega - 2\omega$ fields configuration, let us focus on the harmonic spectra in the energy range 44 - 51 eV. Figure 5 shows the temporal profile of the synthesized attosecond pulse with its x -component, y -component and the Lissajous figure of the total electric field. The pulse shown in Fig. 5(a) has ellipticity as high as 0.88 with ~ 630 attoseconds pulse duration. This elliptical pulse is synthesized by superposing the harmonics in the energy range 44 - 51 eV from the spectra shown in Fig. 1. The high ellipticity is a direct consequence of unequal intensities of the two co- and counter-rotating harmonic components, i.e., D_+ and D_- . In contrast to the co-rotating driving fields, if one considers the counter-rotating driving fields to generate high-

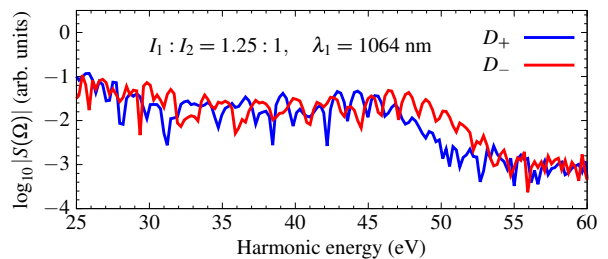


FIG. 4. Same as Fig. 2(b) except the rotation direction of combining fields is reversed. This implies that the D_- harmonic component represented by the red line is now co-rotating with the driving field, while the blue line representing the counter-rotating D_+ harmonic component.

harmonics, the resultant attosecond pulse exhibits ellipticity as low as ~ 0.13 [see Fig. 6]. Thus, co-rotating $\omega - 2\omega$ bicircular fields is a potential way to generate highly elliptical attosecond pulses.

To demonstrate the robustness and universality, we have also synthesized pulses from the spectra shown in Figs. 2(a), 2(b), and 2(d); and the corresponding attosecond pulses are displayed in Figs. 5(b) - 5(d), respectively. The filtered harmonic window is considered near the cutoff region of the respective harmonic spectrum. In all cases, the range of the pulse duration and the ellipticity of the synthesized pulses are $\sim 550 - 600$ attoseconds and $\sim 0.77 - 0.88$, respectively. As expected from the harmonic spectra, the helicity of the generated attosecond pulses is same as the driving laser field. The high ellipticity of the synthesized attosecond pulses proves the potential of the co-rotating $\omega - 2\omega$ fields scheme. Moreover, the absence of rotational symmetry in the co-rotating field configuration translates into the robustness of the generated HHG spectra, wherein small changes in the parameters of the driving fields leave the spectra unaltered.

IV. SUMMARY AND CONCLUSIONS

In summary, we have successfully demonstrated the generation of attosecond pulses with tunable ellipticity via HHG driven by co-rotating $\omega - 2\omega$ bicircular fields. The absence of the dynamical rotational symmetry in the co-rotating $\omega - 2\omega$ fields translates into the generation of the harmonics with same helicity, which leads to elliptically polarised attosecond pulses. It is found that the essential features of the generated harmonics, via co-rotating $\omega - 2\omega$ fields configuration, remain insensitive against variations in laser parameters, such as fundamental driving wavelength, intensity ratio, and the subcycle phase between two fields. Moreover, the effect of the focal averaging is expected to negligible as the attosecond pulses are synthesised using harmonics in near-cutoff region [33]. Thus, it avoids the need for precise adjustments of laser parameters from the experimental perspective. Moreover, the reliance of the polarization properties of the harmonics on driving fields' parameters provides opportunities to shape the polarization of the generated attosecond pulses. The gener-

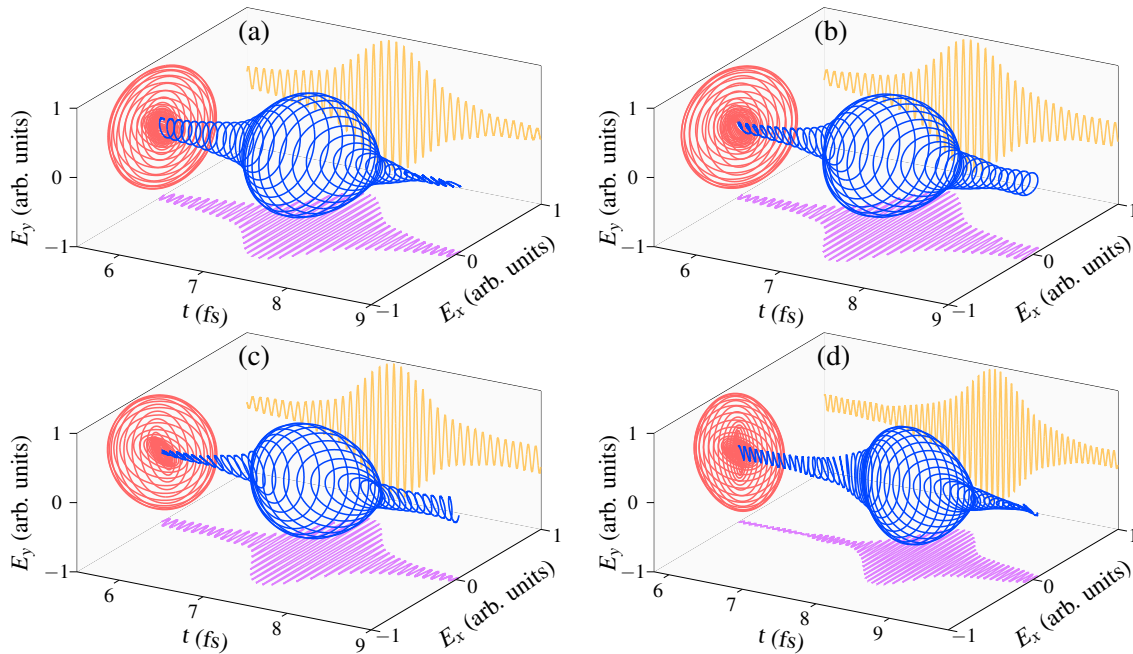


FIG. 5. Temporal profile of the synthesized attosecond pulse (blue line) with its x component (magenta line), y component (yellow line), and Lissajous figure (red line) of the total electric field. Different attosecond pulses are generated by superposing the harmonics near the cutoff region of the harmonic spectra presented in the following figures: (a) Fig. 1, (b) Fig. 2(a), (c) Fig. 2(b), and (d) Fig. 2(d). The synthesized pulses have pulse duration $\sim 550 - 600$ attoseconds, and ellipticity $\sim 0.77 - 0.88$.

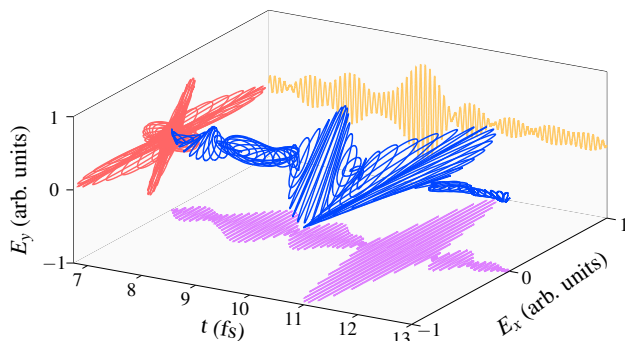


FIG. 6. Temporal profile of synthesized attosecond pulses using counter-rotating $\omega - 2\omega$ driving fields. All other parameters are similar to those used in Fig. 5(a). The synthesized attosecond pulses have ellipticity ~ 0.13 .

ated chiral attosecond pulses can be employed to study chiral-sensitive dynamics on its intrinsic timescales [26–30]. Furthermore, our work can extend to various scenarios, such as current-carrying molecular states, which can further increase the ellipticity of the pulse [44, 45] or different pulse shaping techniques to extend the harmonic cutoffs [46–48].

ACKNOWLEDGMENTS

A. R. H. acknowledges support from Science and Engineering Research Board (SERB) India (CRG/2020/001020). G. D. acknowledges support from SERB India (Project No. MTR/2021/000138).

-
- [1] K. Midorikawa, *Nat. Photon.* **16**, 267 (2022).
 - [2] K. J. Schafer, B. Yang, L. F. DiMauro, and K. C. Kulander, *Phys. Rev. Lett.* **70**, 1599 (1993).
 - [3] P. B. Corkum, *Phys. Rev. Lett.* **71**, 1994 (1993).
 - [4] F. Krausz and M. Ivanov, *Rev. Mod. Phys.* **81**, 163 (2009).
 - [5] P. B. Corkum and F. Krausz, *Nat. Phys.* **3**, 381 (2007).
 - [6] M. Chini, K. Zhao, and Z. Chang, *Nat. Photon.* **8**, 178 (2014).
 - [7] D. Baykusheva, M. S. Ahsan, N. Lin, and H. J. Wörner, *Phys. Rev. Lett.* **116**, 123001 (2016).
 - [8] D. M. Reich and L. B. Madsen, *Phys. Rev. Lett.* **117**, 133902 (2016).
 - [9] T. Bredtmann, M. Ivanov, and G. Dixit, *Nat. Commun.* **5**, 5589 (2014).
 - [10] G. Dixit, O. Vendrell, and R. Santra, *Proc. Natl. Acad. Sci. U.S.A.* **109**, 11636 (2012).
 - [11] O. Neufeld and O. Cohen, *Phys. Rev. Lett.* **120**, 133206 (2018).
 - [12] K. M. Dorney, J. L. Ellis, C. Hernández-García, D. D. Hickstein, C. A. Mancuso, N. Brooks, T. Fan, G. Fan, D. Zusin,

- C. Gentry, P. Grychtol, H. C. Kapteyn, and M. M. Murnane, *Phys. Rev. Lett.* **119**, 063201 (2017).
- [13] S. Long, W. Becker, and J. K. McIver, *Phys. Rev. A* **52**, 2262 (1995).
- [14] H. Eichmann, A. Egbert, S. Nolte, C. Momma, B. Welleghausen, W. Becker, S. Long, and J. K. McIver, *Phys. Rev. A* **51**, R3414 (1995).
- [15] M. V. Frolov, N. L. Manakov, A. A. Minina, N. V. Vvedenskii, A. A. Silaev, M. Y. Ivanov, and A. F. Starace, *Phys. Rev. Lett.* **120**, 263203 (2018).
- [16] R. Rajpoot, A. R. Holkundkar, and J. N. Bandyopadhyay, *J. Phys. B: At. Mol. Opt. Phys.* **54**, 225401 (2021).
- [17] D. B. Milošević, W. Becker, and R. Kopold, *Phys. Rev. A* **61**, 063403 (2000).
- [18] A. Fleischer, O. Kfir, T. Diskin, P. Sidorenko, and O. Cohen, *Nat. Photon.* **8**, 543 (2014).
- [19] O. Kfir, P. Grychtol, E. Turgut, R. Knut, D. Zusin, D. Popmintchev, T. Popmintchev, H. Nembach, J. M. Shaw, A. Fleischer, *et al.*, *Nat. Photon.* **9**, 99 (2015).
- [20] D. B. Milošević and W. Becker, *Phys. Rev. A* **102**, 023107 (2020).
- [21] D. D. Hickstein, F. J. Dollar, P. Grychtol, J. L. Ellis, R. Knut, C. Hernández-García, D. Zusin, C. Gentry, J. M. Shaw, T. Fan, K. M. Dorney, A. Becker, A. Jaroń-Becker, H. C. Kapteyn, M. M. Murnane, and C. G. Durfee, *Nat. Photon.* **9**, 743 (2015).
- [22] P.-C. Huang, C. Hernández-García, J.-T. Huang, P.-Y. Huang, C.-H. Lu, L. Rego, D. D. Hickstein, J. L. Ellis, A. Jaron-Becker, A. Becker, S.-D. Yang, C. G. Durfee, L. Plaja, H. C. Kapteyn, M. M. Murnane, A. H. Kung, and M.-C. Chen, *Nat. Photon.* **12**, 349 (2018).
- [23] G. Dixit, A. Jiménez-Galán, L. Medišauskas, and M. Ivanov, *Phys. Rev. A* **98**, 053402 (2018).
- [24] I. N. Ansari, C. Hofmann, L. Medišauskas, M. Lewenstein, M. F. Ciappina, and G. Dixit, *Phys. Rev. A* **103**, 013104 (2021).
- [25] D. B. Milošević and W. Becker, *Phys. Rev. A* **62**, 011403 (2000).
- [26] T. Fan, P. Grychtol, R. Knut, C. Hernández-García, D. D. Hickstein, D. Zusin, C. Gentry, F. J. Dollar, C. A. Mancuso, C. W. Hogle, O. Kfir, D. Legut, K. Carva, J. L. Ellis, K. M. Dorney, C. Chen, O. G. Shpyrko, E. E. Fullerton, O. Cohen, P. M. Oppeneer, D. B. Milošević, A. Becker, A. A. Jaroń-Becker, T. Popmintchev, M. M. Murnane, and H. C. Kapteyn, *Proc. Natl Acad. Sci. USA* **112**, 14206 (2015).
- [27] R. Cireasa, A. E. Boguslavskiy, B. Pons, M. C. H. Wong, D. Descamps, S. Petit, H. Ruf, N. Thiré, A. Ferré, J. Suarez, J. Higué, B. E. Schmidt, A. F. Alharbi, F. Légaré, V. Blanchet, B. Fabre, S. Patchkovskii, O. Smirnova, Y. Mairesse, and V. R. Bhardwaj, *Nat. Phys.* **11**, 654 (2015).
- [28] Y. Tang and A. E. Cohen, *Science* **332**, 333 (2011).
- [29] E. Hendry, T. Carpy, J. Johnston, M. Popland, R. V. Mikhaylovskiy, A. J. Laphorn, S. M. Kelly, L. D. Barron, N. Gadegaard, and M. Kadodwala, *Nature Nanotechnol.* **5**, 783 (2010).
- [30] D. Baykusheva and H. J. Wörner, *Phys. Rev. X* **8**, 031060 (2018).
- [31] S. Giri, J. C. Tremblay, and G. Dixit, *Phys. Rev. A* **104**, 053115 (2021).
- [32] S. Giri, A. M. Dudzinski, J. C. Tremblay, and G. Dixit, *Phys. Rev. A* **102**, 063103 (2020).
- [33] W. Li, X. Zhu, P. Lan, and P. Lu, *Phys. Rev. A* **106**, 043115 (2022).
- [34] Y. Qiao, D. Wu, J.-G. Chen, J. Wang, F.-M. Guo, and Y.-J. Yang, *Phys. Rev. A* **100**, 063428 (2019).
- [35] N. Rana, M. S. Mrudul, and G. Dixit, *Phys. Rev. Appl.* **18**, 064049 (2022).
- [36] Y. Chen, X. Shen, W. Lan, S. Li, F. Guo, and Y. Yang, *Symmetry* **14**, 519 (2022).
- [37] G.-R. Jia, X.-Q. Wang, T.-Y. Du, X.-H. Huang, and X.-B. Bian, *J. Chem. Phys.* **149**, 154304 (2018).
- [38] R. Rajpoot, A. R. Holkundkar, and J. N. Bandyopadhyay, *J. Phys. B: At. Mol. Opt. Phys.* **53**, 205404 (2020).
- [39] X. Zhang, X. Zhu, X. Liu, D. Wang, Q. Zhang, P. Lan, and P. Lu, *Opt. Lett.* **42**, 1027 (2017).
- [40] X.-X. Huo, Y.-H. Xing, T. Qi, Y. Sun, B. Li, J. Zhang, and X.-S. Liu, *Phys. Rev. A* **103**, 053116 (2021).
- [41] R. Rajpoot and A. R. Holkundkar, *J. Phys. B: At. Mol. Opt. Phys.* **56**, 105402 (2023).
- [42] C. Sanderson and R. Curtin, *J. Open Source Softw.* **1**, 26 (2016).
- [43] O. E. Alon, V. Averbukh, and N. Moiseyev, *Phys. Rev. Lett.* **80**, 3743 (1998).
- [44] X. Xie, A. Scrinzi, M. Wickenhauser, A. Baltuška, I. Barth, and M. Kitzler, *Phys. Rev. Lett.* **101**, 033901 (2008).
- [45] X. Zhang, X. Zhu, X. Liu, F. Wang, M. Qin, Q. Liao, and P. Lu, *Phys. Rev. A* **102**, 033103 (2020).
- [46] A. R. Holkundkar and R. Rajpoot, *Phys. Scr.* **95**, 085607 (2020).
- [47] M. Lara-Astiaso, R. E. F. Silva, A. Gubaydullin, P. Rivière, C. Meier, and F. Martín, *Phys. Rev. Lett.* **117**, 093003 (2016).
- [48] F. Wang, W. Liu, L. He, L. Li, B. Wang, X. Zhu, P. Lan, and P. Lu, *Phys. Rev. A* **96**, 033407 (2017).